DETERMINATION OF AMBIPOLAR RADIAL TRANSPORT FROM THE PARTICLE BALANCE IN THE TMX-U TANDEM MIRROR

S.L. ALLEN, D.L. CORRELL, D.N. HILL,
T.B. KAISER, D.B. HEIFETZ*
Lawrence Livermore National Laboratory,
University of California,
Livermore, California,
United States of America

ABSTRACT. Ambipolar radial transport (equal ion and electron flux) is not directly measured in tandem mirror experiments because the particle flow does not produce a net electrical current. The first absolute measurements of the ionization source in the Tandem Mirror Experiment Upgrade (TMX-U) plasma have been obtained. These have permitted the determination of the magnitude of ambipolar radial transport from the particle balance. Furthermore, comparisons of the source measurements with a Monte Carlo neutral transport code have shown reasonable agreement. Measurements of the particle balance under several operating conditions are presented. For some of these cases, the ambipolar radial transport is smaller than the other measured losses.

1. INTRODUCTION

Particle confinement in a linear tandem mirror fusion device involves the control of both axial and radial losses. Previous tandem mirror experiments, such as TMX at the Lawrence Livermore National Laboratory (LLNL) [1], have obtained axial particle confinement times greater than those obtained in a single mirror by using axial potentials. In this machine, the axial confining potential ϕ_c was established by the density ratio between the end cell and the central cell [2]: $\phi_c = T_e \ln (n_p/n_c)$, where n is the electron density and the subscripts p and c refer to the end plug and to the central cell. Present tandem mirror experiments such as the upgrade of TMX, called TMX-U, use a thermal barrier configuration [3] to establish the axial confining potential. In this case, both potentially and magnetically confined electrons are created, allowing the density in the central cell to be greater than that in the end cells. This configuration is advantageous for reactor designs in that the central cell is the fusion producing region. Long axial confinement times (about 50–100 ms) have been achieved in thermal barrier experiments on TMX-U [4] and GAMMA-10 [5]. The establishment of long axial confinement times revealed the next important particle loss: *non-ambipolar* radial transport, consisting of *unequal* ion and electron radial fluxes [6, 7]. The non-ambipolar radial ion flux in a tandem mirror is neutralized by an axial electron flux to the end wall of the machine; the electric circuit is completed by the metal vacuum vessel. In TMX-U, reduction of the measured non-ambipolar losses has been achieved by electrically isolating the end walls [8]; to further minimize these losses, other recently built tandem mirror machines have included axisymmetric magnetic fields [5, 9]. Scaling of the non-ambipolar radial confinement time has been examined in detail both in GAMMA-10 [10] and in TMX-U [7, 11].

Recently, we have investigated the particle balance of the TMX-U plasma to ascertain whether *ambipolar* particle losses are present (i.e. the case with *equal* ion and electron radial fluxes). Unlike non-ambipolar radial losses, ambipolar radial losses do not have an associated net electrical current and hence are not detected by the particle current measurements normally used for axial and non-ambipolar radial losses. We describe here the measurement of the known contributions to the particle balance equation in the TMX-U plasma. In particular, we discuss the first direct measurement of the total ionization source.

A detailed explanation of the operation of the TMX-U experiment is outside of the scope of the present discussion and is presented elsewhere [12, 13].

* Princeton Plasma Physics Laboratory, Princeton Univ., Princeton, NJ, USA.

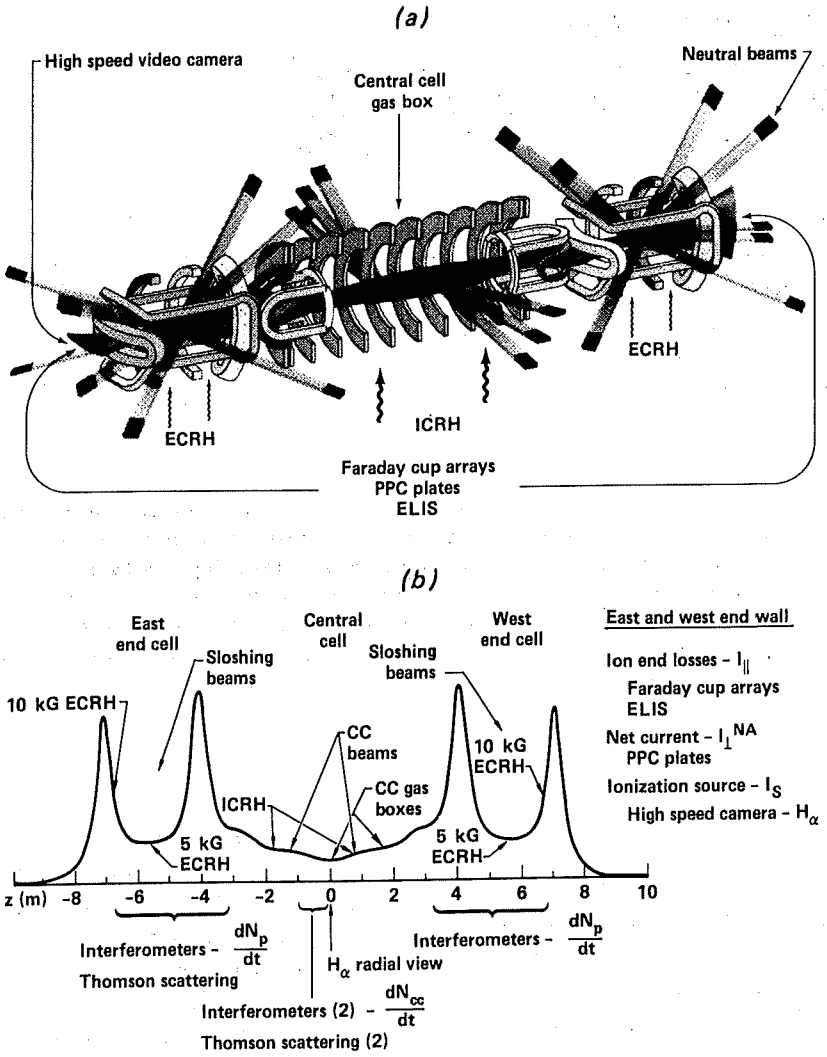

FIG. 1. (a) Schematic of the TMX-U device, showing the ECRH, ICRH and neutral beam heating systems. Only the gas box in the midplane of the central cell was used for this study. (b) Magnetic field profile of TMX-U. Located at each end wall are the diagnostics used to measure the particle balance: Faraday cups to measure $I_{||}$, plasma potential control (PPC) plates to measure $I_{\perp}^{NA}$, and a high speed camera to mesure I_S. The interferometers used to calculate the plasma buildup term are shown in the central cell and the end plugs. Note that the non-uniform magnetic field causes the plasma cross-section to be circular in the midplane of the central cell and the end cells; the cross-section is elliptical in the transition region and at the end wall.

For reference, a schematic of the TMX-U device is shown in Fig. 1(a). The magnetic field profile and the locations of the particle confinement diagnostics are shown in Fig. 1(b). Briefly, TMX-U uses a combination of electron cyclotron resonance heating (ECRH) in the end cells, ion cyclotron resonance heating (ICRH) at two locations in the central cell, and neutral beam injection in both the end plug and the central cell regions to create a plasma. Particle confinement in the thermal barrier mode is achieved by a combination of the magnetic field and the plasma potential. Measurements of plasma potentials and their relationship to the overall confinement in TMX-U are presented in Ref. [14]. For the present discussion, it is important to note in Fig. 1 that the diagnostics used to measure the particle confinement are located at each end of the machine, and the gas injection system (gas box) that is used to fuel the plasma is located in the central cell.

The gas box is an annular tube that contains four gas valves to provide nearly symmetric gas injection.

The paper is organized as follows: Section 2 describes the particle balance equation and the diagnostics used to measure the particle losses. Section 3 presents the measurement of the particle source and a comparison with model predictions from a Monte Carlo neutral transport code called DEGAS [15]. Section 4 presents the particle balance measurements under three specific operating conditions and discusses the associated measurement errors. Section 5 summarizes the particle confinement time measurements to date on TMX-U, and Section 6 follows with concluding remarks.

2. PARTICLE SOURCES AND LOSSES IN TMX-U

2.1. The particle balance equation

The particle sources and losses are shown schematically in Fig. 2. Only one end of the TMX-U machine is shown, but the diagnostic measurements are obtained from both ends. The ion particle balance equation that connects these terms is obtained from the usual particle continuity equation. Impurities have been neglected because spectroscopic measurements [16] have shown that the concentrations are low, i.e. $Z_{eff} \simeq 1$. This simplification produces the particle balance equation:

$$q\frac{dN}{dt} = I_S - I_\parallel - I_\perp^{NA} - I^A \qquad (1)$$

where q is the electron charge, N is the total number of plasma particles, I_S is the ionization plasma source current, $I_\parallel$ is the axial ion loss current, $I_\perp^{NA}$ is the radial non-ambipolar loss current and I^A is the residual loss current required to balance the equation. A positive I^A is attributed to outward ambipolar losses or measurement errors (for example errors resulting from incomplete radial or azimuthal profile measurements of particle losses). These measurement errors will be discussed in detail for each term in the equation. Although Eq. (1) is valid for a plasma column of any radius, we will focus on the plasma core (central cell radius $r \leq 10$ cm) for several reasons. First, the TMX-U magnet set limits the radial field of view of the H_α camera viewing along the plasma axis. This means that a full two-dimensional view of the plasma column (and hence the ionization source I_S) is possible only for a core region of 10 cm radius. Measurements outside of this radius are possible, but azimuthal symmetry must be assumed for I_S because only one sector of the plasma column is viewed. Second, H_α photons can be correlated fairly easily with atomic ionization, but molecular contributions are more difficult to estimate. Because of the attenuation of molecular neutrals from the plasma boundary to the core, the influence of molecular deuterium on the ionization source I_S is the smallest in the core region. This fact has been verified with the Monte Carlo neutral transport code DEGAS and is described in Section 3.2. Finally, the plasma core is the main region of interest for particle confinement studies. Therefore, we define the particle currents in Eq. (1) to be for the plasma core, $r \leq 10$ cm. We now describe the measurement of each term in the particle balance equation, Eq. (1).

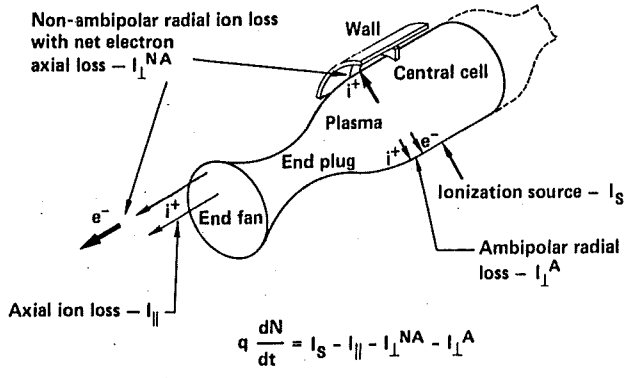

FIG. 2. Particle sources and losses in a tandem mirror plasma. The axial ion loss $I_\parallel$ is measured with Faraday cups equipped with electron repeller grids. The non-ambipolar radial loss $I_\perp^{NA}$ is measured by the net axial electron current. The ionization source I_S, concentrated near the gas injection system in the central cell, is measured by a high speed video camera. The particle balance equation is used to determine the amount of ambipolar transport I^A that is present.

2.2. Measurements of parallel ion losses, $I_\parallel$

The term $I_\parallel$ is obtained from measurements of the axial ion loss current as a function of position. Most of the measurements are obtained from Faraday cup arrays located on each end wall (shown in Fig. 3). Each detector is equipped with a negatively biased screen (−3 kV) to repel electrons. The local end-loss current density $j_\parallel$ is obtained by dividing the collected

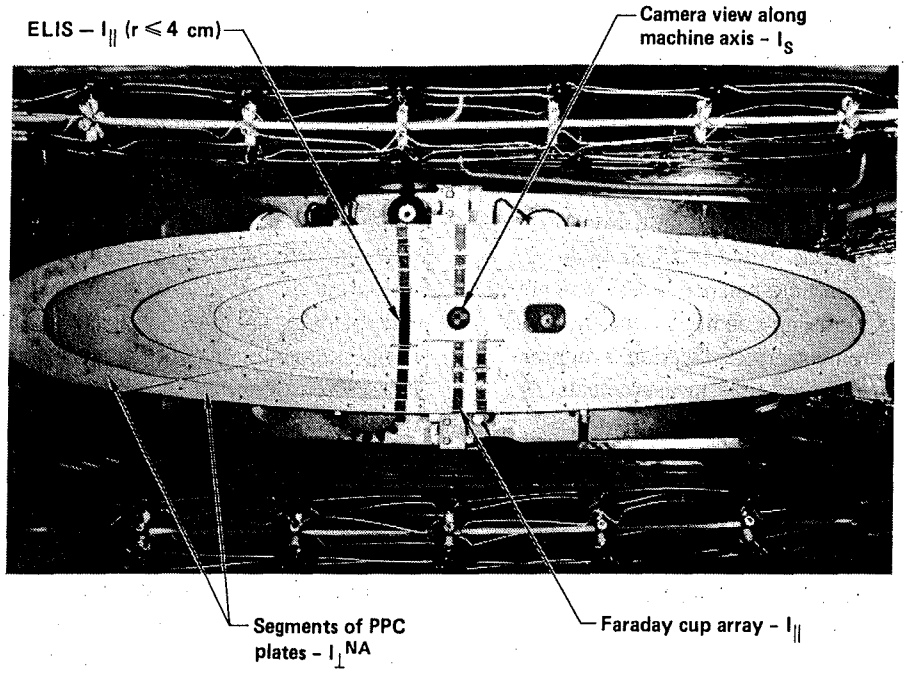

FIG. 3. Picture of the TMX-U end wall. The (vertical) array of Faraday cups to measure $I_{\|}$ is located behind screens in the PPC plates. The ELIS measures the on-axis ion end losses as a function of mass and energy to make sure that the Faraday cup arrays are not influenced by high energy electrons. The segmented PPC plates are elliptical at the end wall and correspond to circular flux tubes in the central cell. The camera views the ionization source in the central cell through a small hole in the centre of the plates.

ion current by the detector area. For a completely circular plasma, the current density is then integrated to obtain the total ion loss current as a function of radius. However, the quadrupole magnet geometry in the end cells of TMX-U causes the circular flux tube in the central cell to become highly elliptical at the end wall. For low beta plasmas, the vacuum magnetic field is used to flux-map the end wall measurements to the central cell; the flux tube is labelled by the radius of the corresponding circular central-cell flux tube. For most cases, a one-dimensional Faraday cup array is used, azimuthal symmetry is assumed and $I_{\|}$ is obtained by integration (with straight line interpolation between the data points). For some data sets, two-dimensional Faraday cup arrays were used to compute $I_{\|}$. Comparison of these data with the one-dimensional data shows that the typical error in $I_{\|}$ resulting from the assumption of azimuthal symmetry is of the order of 20%. When this error is coupled with the possible calibration errors in the amplifiers and data recorders, the total estimated error in $I_{\|}$ is of the order of 25%.

Another possible error in $I_{\|}$ is caused by energetic electrons (≥ 3 keV) leaking through the Faraday cup repelling grids and neutralizing a portion of the ion current. An end loss ion spectrometer (ELIS) [17] at each end of TMX-U measures the ion loss current versus energy and mass near the plasma axis ($r \leq 4$ cm). This instrument is an E$\|$B analyser and is therefore insensitive to an incoming electron current. This provides an on-axis verification that $I_{\|}$ from the Faraday cup arrays is correct. For the experimental conditions discussed in this paper, we found that the ELIS diagnostic agrees well with the current density measured by the Faraday cups.

2.3. Measurements of non-ambipolar radial losses, $I_{\perp}^{NA}$

As discussed above, the radial fluxes of ions and electrons need not be equal in a tandem mirror. In most cases observed in TMX-U, more electrons than ions escape to the end wall so that the net axial current

is negative. This net negative axial current balances an outward radial flux of ions. Under these conditions, we can define $I_{\perp}^{NA}$ to be identical with the absolute value of the escaping net electron current. The net current is measured directly by a set of elliptical plasma potential control (PPC) plates, shown in Fig. 3, which map to circles in the midplane of the central cell. This array of plates is composed of several electrically independent segments so that the radial and azimuthal dependence of the net current can be studied. In addition, each PPC plate can be isolated from ground (10 kΩ or 1 MΩ), grounded, or switched from one mode to the other during the shot. The switching times are pre-programmed before the plasma shot. This flexibility is necessary to efficiently study non-ambipolar radial transport, which is discussed in detail in Ref. [7].

The non-ambipolar radial loss current $I_{\perp}^{NA}$ is obtained by adding up the current corresponding to the core flux tube, which includes the inner three rings of plates. As expected, it is observed experimentally that the current is greatly reduced when the PPC plates are isolated from ground. Also, it should be noted that when the plates are completely isolated from ground and no $I_{\perp}^{NA}$ current is measured, any residual non-ambipolar losses caused by magnetic field errors or non-axisymmetric potential profiles are, by definition of Eq. (1), included in I^{A}.

Since the current is integrated automatically by the PPC plates, the uncertainty in $I_{\perp}^{NA}$ originates primarily from the calibration of the amplifiers and digitizers. However, if magnetic field errors are present, the elliptical flux tubes corresponding to the PPC plates on the end wall map to a different central-cell flux tube, resulting in an effective error in $I_{\perp}^{NA}$. For this reason, we have performed magnetic field alignment studies by placing an electron beam in the central cell and determining its location on the end wall by measuring the current collected on the PPC plates. Small trim coils are used to make minor adjustments in the flux tube mapping. Typical errors are small, of the order of less than 1 cm error for mapping a central-cell flux tube of 25 cm to the end wall. This error is smaller for the core of the plasma, and we estimate the total error in $I_{\perp}^{NA}$ to be of the order of 10%.

2.4. Measurements of particle buildup, dN/dt

The term dN/dt is the time rate of change of the total number of particles; it is calculated from line density measurements. Several microwave interferometers located in the central cell and end cells are used to obtain rough profiles of axial and radial electron density. Thomson scattering data in one end plug and in the central cell are also used for point density measurements at two radial locations. At electron densities above 10^{12} cm^{-3}, we have also used a beam attenuation diagnostic [18] to measure radial line density profiles. For the data presented here, a Gaussian radial profile was used for the central cell with a 20 cm 1/e radius. This radius is then flux mapped into the end cells. These profiles are consistent with the data obtained from the multi-chord beam attenuation measurements. Under many conditions, the central-cell ion distribution is isotropic, and interferometers near the end of the central cell indicate that the axial density profile is flat. Thus, the axial density profile is assumed constant with an effective cylindrical flux tube length $L_c = B_c \int (dl/B)$, which is 500 cm for the central cell and 200 cm for the end plugs. This representation of the density profile allows the dN/dt term to be calculated by $Vd(\hat{n})/dt$, where V is the core plasma volume (constant in time) and $\hat{n}$ is the on-axis density derived from the measured line density. Calculations are performed from separate measurements in each end plug and in the central cell. The particle buildup term has the largest uncertainty of all the terms in the particle balance equation. However, it is possible to minimize this error by selecting operational modes where this term is small (i.e. when the density reaches a steady state value). This is often the case after the first 20–30 ms of the plasma pulse. Errors can be present when the density is changing rapidly; this case is discussed in detail in Section 4.3.

3. H_α MEASUREMENTS FOR I_S AND COMPARISONS WITH THE DEGAS CODE

3.1. Two-dimensional H_α measurements

The term I_S is obtained from absolutely calibrated two-dimensional measurements of H_α emission. Figure 4 shows a cross-section of TMX-U and the locations of the cameras: one camera, called the end-view camera, views the plasma parallel to the plasma column from one end of the machine; the other camera, the side-view camera, has a view that is perpendicular to the plasma column. The end-view camera capitalizes on the unique linear geometry of TMX-U: the view automatically integrates the axial emission profile. In contrast to H_α measurements on tokamaks, which require a large number of toroidal

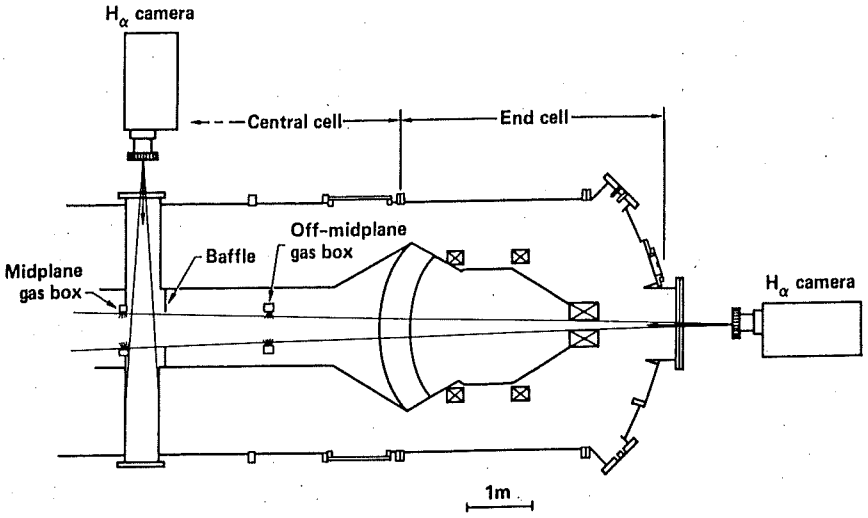

FIG. 4. Locations of the end-view and side-view cameras. The side-view camera shows that most of the ionization source is near the gas box in the circular portion of the central cell. The end-view camera automatically obtains the axial integral of the ionization source as a function of radius. Other cameras have been used to show that the ionization source is small in the end cells. Only the midplane gas box was used for this study.

locations, a single camera on TMX-U can obtain the axially integrated H_α emission as a function of radius. In practice, however, there are limitations to the axial integration obtained by the end-view camera. One limitation is the depth-of-field of the camera's optical system. In the TMX-U case, this was experimentally measured and found to be greater than the length of the central cell. Another limitation is that the TMX-U flux tube is not circular, so that if a large amount of ionization originates from a highly elliptical region (for example in the transition region between the central cell and the end cells) it will be attributed to the wrong flux tube. The side-view camera is therefore used to measure the axial extent of the emission near the gas box (where the plasma cross-section is circular) to verify that the end-view camera is measuring the total source.

All of the end-view camera measurements used a high speed camera system (Spin Physics SP-2000) capable of full-frame time resolution of 0.5 ms per frame; partial frames could be obtained in one-sixth of this time. For most TMX-U plasmas, 1 ms per frame was typically used, with some data obtained at 5 ms per frame and 0.5 ms per frame. The bandpass of the interference filter mounted on the camera had a full width at half maximum (FWHM) of 30 Å with a central wavelength of 6561 Å. The bandpass of the filter was chosen to be sufficiently narrow to minimize the mixing of other plasma emissions with the H_α line, but sufficiently broad to match the collimation of the optical system so that the sensitivity of the system was not a function of angle (i.e. rays from the plasma were nearly parallel to the filter). The sensitivity of the system was absolutely calibrated with a tungsten ribbon lamp using standard techniques established by the National Bureau of Standards [19]. All the optical components used in the TMX-U experiment were in place during the calibration. These measurements were repeated in the course of the experiment to ensure that the calibration was stable.

Most of the side-view measurements were made with several CCD cameras (SONY-XC38) operating at conventional video rates of 60 frames per second. These portable cameras are more sensitive than the high speed camera, so they were well suited to verify the small emission rates in the end plugs. They also provided a good representation of the fuelling near the gas injection system during the steady state portion of the discharge. The camera data were recorded on standard video tape and then digitized; the sensitivity of these cameras was also absolutely calibrated.

The experimental data from the side-view cameras in the central cell show that most of the H_α emission occurs near the gas injection system, with a very sharp

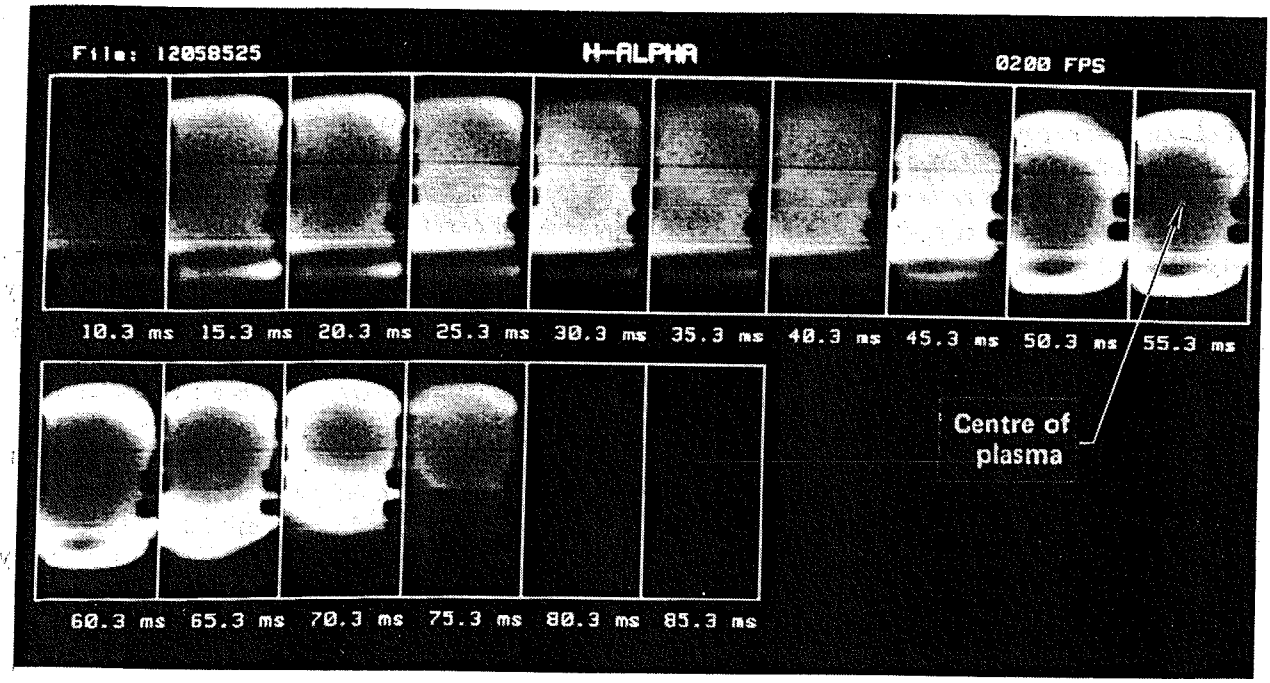

FIG. 5. Sample data from the high speed H_α camera. A time resolution of 5 ms per frame was used for these data. The centre of the plasma is shown on one of the frames. A full two-dimensional view of the core of the plasma is obtained. Outside of the core, the field of view is cut off by the TMX-U magnets. The plasma buildup occurs from 0 to 25 ms, then the sloshing beams are turned on at 25 ms. The plasma density increases over the period from 40 to 50 ms, and the total profile becomes more peaked at the edge. The data from the core of the plasma (approximately the dark circle in the frame labelled 55.3 ms) are analysed in the present discussion.

axial fall-off. Therefore, this emission is within the depth-of-field of the end-view camera. In addition, we have made side-view measurements in both end plugs to verify that their contribution to I_S is small (less than 10% for most conditions). In this way, we have used the side-view cameras to determine experimentally that the data from the end-view camera are a good measure of the axially integrated H_α source.

Several frames of data from the end-view camera are shown in Fig. 5; a time resolution of 5 ms per frame was used for these data. The plasma centre is indicated in the figure, and at the top of each frame is the edge of the gas box, which is located at a central-cell flux tube of 25 cm. The sides of the view are cut off by the TMX-U end-cell magnets; the open horizontal aperture corresponds to a flux tube of 10 cm radius. Thus, a full two-dimensional measurement is obtained for the plasma core, but only a sector of the plasma cross-section is obtained for larger radii. Between plasma shots, the emission data are digitized from the high speed magnetic tape and stored on disk. The emission corresponding to the core flux tube is then obtained by adding up the signals from the corresponding camera pixels. The next step is the conversion of the measured H_α emission to an ionization source rate. For most cases, this is a straightforward correction obtained by multiplying the total emission by an atomic physics factor R, which is essentially the branching ratio between electron impact ionization and electron impact excitation followed by H_α emission. This factor involves the ratio between two cross-sections; for the TMX-U core plasma, it is insensitive to electron temperature and density. For the typical core plasma conditions of TMX-U (central-cell density in the 10^{12} cm^{-3} regime and electron temperature of $\simeq$100 eV), R = 11 ionizations per photon is calculated using the data in Ref. [20]. There are variations of about $\pm$10% over the usual range of plasma conditions. The resulting I_S is then transferred to the main TMX-U database for comparison with the other terms in the particle balance.

Direct molecular processes are not included in the calculations of Ref. [20], so the ionization rate obtained with the factor R is from *atoms* that are ionized. Simple analytical models suggest that most of the molecules are attenuated before they reach the

TMX-U plasma core and that therefore most of the ionization in the core is due to atoms. We have used the DEGAS code, which is a detailed Monte Carlo model of neutral transport, to determine the influence of molecules on the core ionization rate; the details of this modelling are discussed in Section 3.2. The DEGAS code independently calculates the atomic H_α emission rate and the ionization rate, so that the R-factor can be calculated for various plasma parameters. For the core of the TMX-U plasma, it is found that $R = 11 \pm 10\%$, in agreement with the (atomic ionization) calculations of Ref. [20]. For shots at lower electron density and temperature (e.g. $n_e \leq 5 \times 10^{11}$ cm^{-3} and $T_e \leq 40$ eV), and also at the edge of the plasma, molecules do influence the ionization. Semi-empirical models of emission in the presence of molecules have been included in DEGAS, indicating that R may be as large as 20–30, in agreement with other observations [21]. In summary, the DEGAS calculations indicate that only *atomic* ionization is important in the core of the TMX-U plasma for most plasma conditions, and the influence of molecules is important at the plasma edge.

3.2. Comparison of H_α measurements with DEGAS

As discussed in Section 3.1, the side-view cameras showed that most of the H_α emission was localized near the gas injection system in the central cell. The Monte Carlo neutral transport code DEGAS was used to model this feature and to calculate the ionization rate from the H_α emission rate to verify that the source of the ionization in the plasma core was primarily from atoms. The computer code is described in detail in Ref. [15]. This particular application of DEGAS to TMX-U employs a two-dimensional Monte Carlo model of the neutral transport. The code calculates all the dominant reactions between the plasma and neutrals, such as charge exchange, electron and ion impact ionization, molecular dissociation and recombination. In addition, a wall interaction model is included to calculate quantities such as wall reflection.

The most important input to the code is the TMX-U geometry. Engineering drawings have been used to obtain the exact dimensions and materials that surround the TMX-U plasma. A sample input grid is shown in Fig. 6; this is effectively a section through the axis of the machine and azimuthal symmetry is assumed. Note that the gas box (the gas injection system), ICRH antennas and baffles are included. For this particular case, we have focused on the central-cell region of TMX-U. The flux tubes are nearly circular in this region, which simplifies the model. Near the ends of the axial grid ($Z \geq 200$), the radial computer grid has been adjusted to account for the slightly elliptical flux tubes. The actual TMX-U machine consists of three concentric chambers (see Ref. [22] for a detailed explanation and drawings): the outer two regions provide differential pumping and are analogous to neutral beam lines in other devices; the inner chamber surrounds the plasma. We have modelled this geometry by concentrating on the inner plasma region, replacing the outer two pumping regions by an adjustable gas input from the beam lines. This is a reasonable simplification of the real geometry because the measured gas input from the gas box is at least 10–20 times that of the beam lines. In the centre of the grid (near $Z = 0$), there is effectively an exit for particles because the inner plasma chamber is connected directly to the outer wall of the machine. This duct is gettered and cooled to liquid nitrogen temperature.

The background plasma conditions are also input into the model, together with the gas flow rates. Gaussian radial profiles with a 1/e width of 20 cm (see Section 2.4) were used for the electron density, ion density and electron temperature. For the particular shot modelled, the measured on-axis central-cell quantities were: $n_e = 2.5 \times 10^{12}$ cm^{-3}, $T_e = T_i = 100$ eV, and the gas box flow rate was 20 torr·L·s^{-1}. The code was run with a large number of particles (10 000) so that sufficient statistics were obtained for the desired outputs. The code calculates a large number of quantities, including the radial and axial profiles of atomic and molecular density and pressure, and the ionization rate. The code also has an atomic physics package that calculates the H_α emission directly.

Shown in Fig. 7 is the total H_α emission density as a function of radius and axial position, calculated from DEGAS for TMX-U conditions. The baffles and ICRH antennas are projected on the top right-hand part of the figure for reference. Note the rapid decay of the emission away from the gas box, a decrease of more than two orders of magnitude. Figure 8 shows an axial cut of the intensity near the plasma axis (-2 cm $\leq r \leq 2$ cm); the normalized DEGAS output and the data from the side-view camera are compared. The DEGAS output has been divided by 2, to bring the two curves into agreement. With this adjustment, the agreement is quite good, and these results demonstrate that the emission is localized very close to the gas box. A detailed discussion of the comparison of axial and radial H_α profiles with DEGAS is presented in Ref. [23].

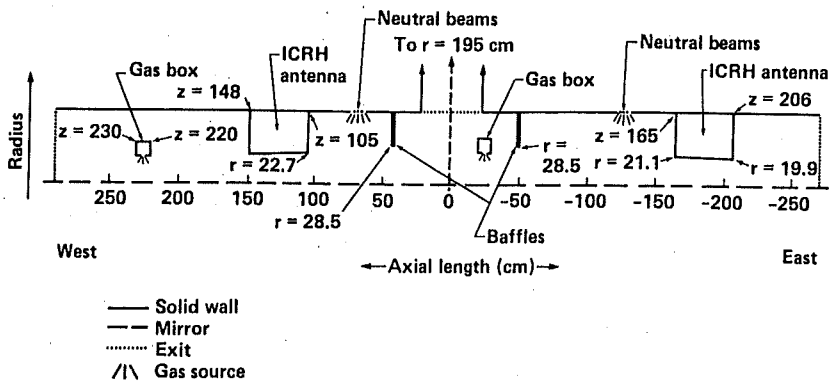

FIG. 6. Geometrical grid used for DEGAS to model TMX-U. An axial segment through the machine is shown; azimuthal symmetry is assumed. The gas box, ICRH antennas and other interior details of TMX-U have been included in the model. The outer two annular vacuum regions have been modelled by adjusting the gas input from the neutral beams.

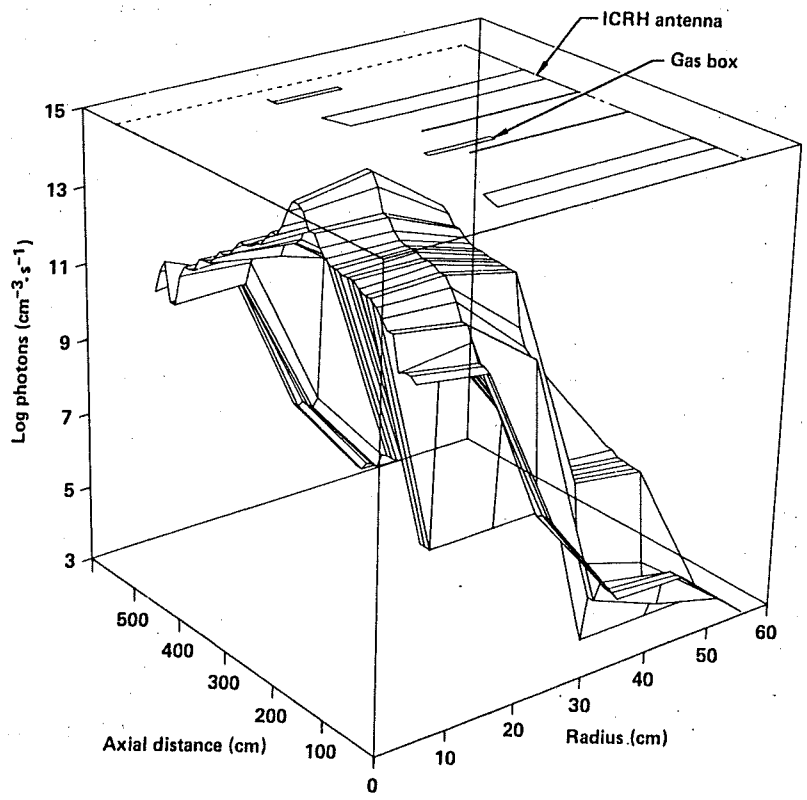

FIG. 7. Total H_α emission density from DEGAS. Note that the emission falls off rapidly away from the gas box. The outlines of the gas box, baffles and other structures shown in Fig. 6 are shown on the upper right-hand side of the box for reference.

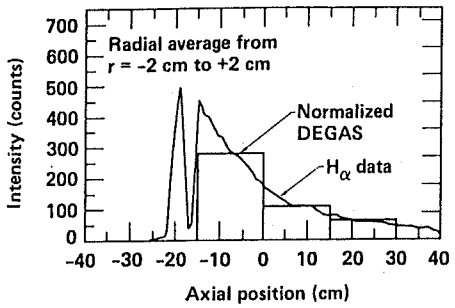

FIG. 8. Comparison of the axial profile of the H_α data from the side-view camera in the central cell at the gas box with calculations from DEGAS; note the very sharp drop-off in the emission, showing a highly localized source. The data have been normalized near the midplane gas box (i.e. at about -10 cm) to demonstrate the shape of the axial profile.

We have also compared the DEGAS results with ionization gauge measurements of the neutral pressure [24]. These gauges are located close to the plasma and are absolutely calibrated with the TMX-U magnetic field. Between each gauge and the plasma there is a neutralizer plate so that the pressure measured by the gauge is a molecular neutral pressure (with the ambient wall temperature). The DEGAS neutral densities are then converted to a pressure with this wall temperature for comparison with the data. We find that the agreement is similar to that in the H_α case; the DEGAS results are within a factor of two.

Certainly, many other comparisons between the data and the DEGAS code are possible. We have not attempted to iterate the code model to obtain better than a factor-of-two agreement with the data because of the inherent experimental uncertainties, particularly the gas flow rate into the gas box. For the present discussion, the code has demonstrated — in agreement with the experimental data from the side-view camera — that the end-view camera *does* integrate the majority of the emission because of the localization of the source; the end cells have been independently checked with the side-view cameras and the emission is low. The DEGAS code has also been used to check that the influence of molecules on I_S in the core of the plasma is small.

4. PARTICLE BALANCE MEASUREMENTS IN TMX-U PLASMAS

Using the above techniques for determining the terms $I_\parallel$ (axial losses from the Faraday cup arrays), $I_\perp^{NA}$ (non-ambipolar radial losses from the PPC plates), I_S (ionization source from H_α data) and q dN/dt (rate-of-change of the total number of plasma particles) in Eq. (1), we performed particle balance measurements during several months of TMX-U operation under various plasma conditions. Under many operating conditions, the particle balance equation could be satisfied with a very small I^A. However, finite I^A was identified for certain plasma conditions. To facilitate the discussion of these various cases, we will define a particle current:

$$I_T \equiv I_\parallel + I_\perp^{NA} + q\frac{dN}{dt}$$

The particle balance equation can then be written in the simple form:

$$I^A = I_S - I_T$$

The convenience of this notation is that we can consider three experimental cases where one term dominates I_T: Case 1: $I_\parallel$ is the largest term (large axial losses), Case 2: $I_\perp^{NA}$ is the largest term (small axial losses), and Case 3: q dN/dt dominates I_T (plasma buildup). Cases 1 and 3 have small I^A, and Case 2 is one example of finite I^A. As noted above, the experimental uncertainties are different for each case.

4.1. Case 1: $I_\parallel$ dominates I_T — small I^A

The plasma conditions for this case are that $I_\parallel$ is large (i.e. no axial 'plugging') and both q dN/dt and $I_\perp^{NA}$ are very small after the initial plasma buildup.

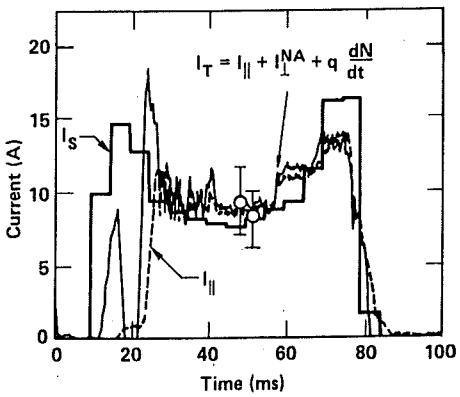

FIG. 9. Experimental Case 1: $I_\parallel$ is the largest term in I_T (i.e. no axial plugging) and I_S is equal to I_T so that I^A is small. Experimental error bars are shown for I_S and I_T.

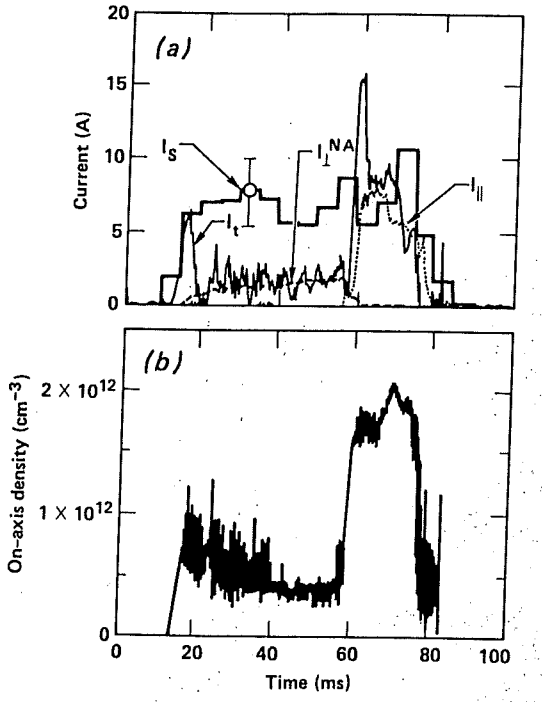

FIG. 10. Experimental Case 2: $I_\perp^{NA}$ is the largest term in I_T, and I_S and I_T are not equal so that finite I^A is present. (a) Sources and losses; finite I^A is present from 20 to 60 ms. The uncertainty in I_S is shown; the 10% error in I_T due to $I_\perp^{NA}$ is approximately 0.1 A. After 60 ms, the conditions are similar to Case 1. (b) Oscillation in electron density. Note that the density derived from the microwave interferometer is noisy over the period of finite I^A. Fourier analyses of these data indicate a fluctuation frequency near 7 kHz.

Representative data for this case are shown in Fig. 9, where $I_\parallel$, I_T and I_S are compared. The time resolution of the video camera was 5 ms per frame for this shot. Note that the curves for $I_\parallel$ and I_T are nearly identical after the initial buildup, showing that $I_\parallel$ is the dominant term in I_T during the steady-state portion of the shot. The ionization source I_S agrees well with I_T after the initial phase of the shot ($t \leq 25$ ms). The disagreement early in time presumably results from changes in the radial density profiles during the plasma buildup (recall that a constant profile is used to calculate the particle buildup term). After this initial phase, the good agreement between I_S and I_T indicates that the term I^A is small for these conditions. The experimental errors to be compared under these conditions are a 25% error in I_S and a 25% error in I_T (due to the error in $I_\parallel$); representative error bars are shown in Fig. 9. This case provides a convenient calibration case and permits a check of the validity of the measurement. We were also able to vary the gas fuelling and to obtain measurements at 60–70 A of particle current (note that I_S in Fig. 10 is 10–15 A); I_S and I_T were nearly equal under these conditions. This scaling suggests that there is no systematic error in the experimental measurements.

4.2. Case 2: $I_\perp^{NA}$ dominates I_T — finite I^A

For many experimental configurations, we found that I^A was small, as in Case 1. However, we did observe finite ambipolar transport under certain plasma conditions. Shown in Fig. 10(a) are the particle currents for I_S, I_T, $I_\perp^{NA}$ (0–60 ms) and $I_\parallel$ (60–80 ms). At the very beginning of the shot, there is fairly good agreement between I_S and I_T. After 20 ms, the total particle loss is nearly equal to $I_\perp^{NA}$; the fluctuation in the I_T curve is due to the oscillation in the electron density shown in Fig. 10(b). From 20 to 60 ms, $I_\parallel$ is small (strong axial plugging), but there is a large discrepancy between I_S and $I_\perp^{NA}$, denoting a significant I^A. The experimental errors to be compared during this period are the 25% error in I_S and the 10% error in I_T resulting from the uncertainty in $I_\perp^{NA}$. A representative 10% error bar is shown for I_S; the error bar for $I_\perp^{NA}$ is difficult to represent on the figure because it is of the order of 0.1 A. After 60 ms, the $I_\perp^{NA}$ term goes to zero and the principal loss current is $I_\parallel$. During this period, with conditions similar to those in Case 1, I_T and I_S agree well, again denoting small I^A. Under these conditions, on a series of shots the transition from finite I^A to small I^A and the accompanying density rise occurred spontaneously at various times during the 80 ms plasma duration.

Several shots under Case 2 conditions were studied to determine the cause of the finite I^A most of these shots, the microwave interferometer signals in the central cell were noisy over the period of finite I^A and became quieter over the period of agreement between I_S and I_T. Fourier analysis of the interferometer traces often indicated a spectrum of fluctuations centred near 7 kHz, which was particularly evident on the channel at r = 13 cm in the central cell. To date, we have not been able to conclusively identify the source of this mode and thereby, presumably, the source of the ambipolar transport. Detailed experiments and data analyses are currently in progress; in particular, data from radiofrequency (RF) probes at the edge of the plasma are being analysed [25]. However, we have been able to empirically minimize both the fluctuations and I^A by careful control of the ICRH

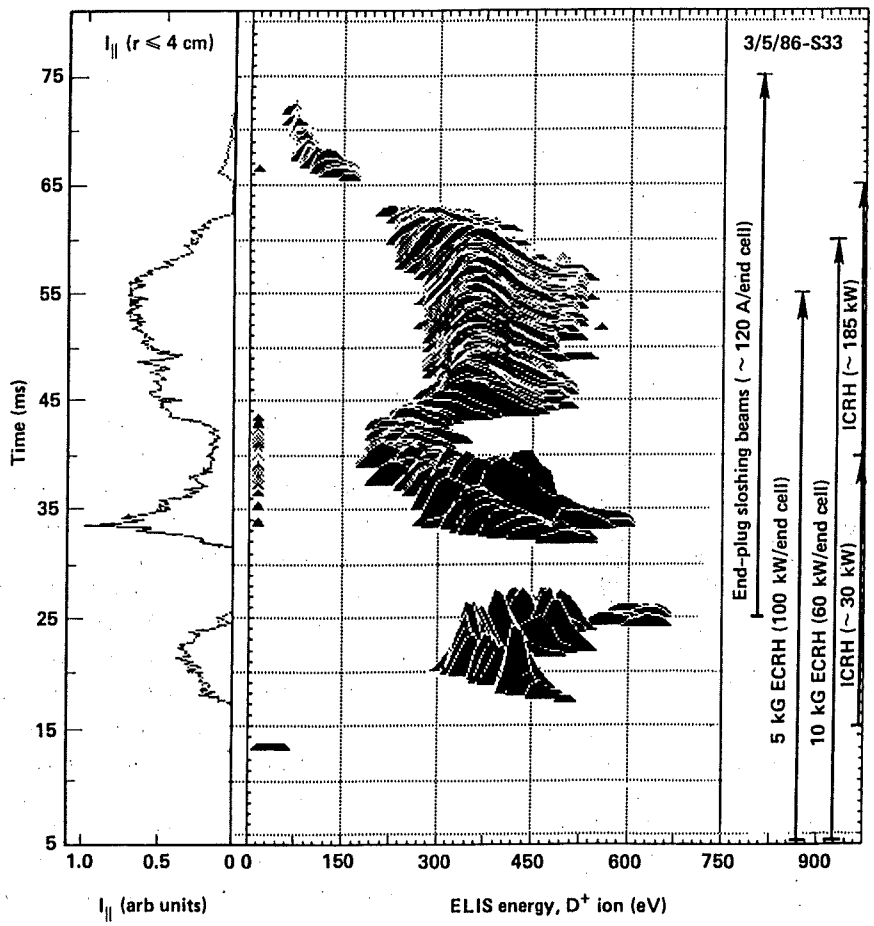

FIG. 11. Experimental Case 3: q dN/dt is the largest term in I_T. The ion losses as a function of energy from the ELIS diagnostic are in the centre of the figure. On the right-hand side, the timing of the heating and fuelling systems for this shot is presented. On the left-hand side, the integral of the ELIS current is shown. Note the reduced axial losses starting at 25 ms.

power in the central cell and the gas fuelling. While the absolute threshold of ICRH power and fuelling rate seems to be a complicated function of plasma conditions, a general observation is that decreasing the ICRH power or increasing the fuelling rate usually aids the return to conditions with small I^A. Although the exact cause of the rise of I^A is uncertain at present, these data illustrate the importance of particle balance measurements in a tandem mirror, particularly the measurement of the ionization source to obtain I^A.

4.3. Case 3: Particle buildup q dN/dt dominates I_T

We also performed particle balance measurements over periods during which both $I_{\parallel}$ and $I_{\perp}^{NA}$ were small. Under these conditions, the largest term in I_T was q dN/dt. The plasma heating systems for these conditions were in the normal thermal barrier configuration discussed in Ref. [4]. The ECRH systems were operating at approximately 100 kW at the B = 5 kG location near the midplane of the plug where the fundamental ECRH resonance for 28 GHz occurs, and at 60 kW at the B = 10 kG location where the second harmonic resonance occurs. ICRH heating was used in the central cell (see Fig. 1 for axial locations). The timing of the heating systems is shown on the right-hand side of Fig. 11, together with the ELIS measurement of the on-axis ion end-loss current as a function of energy. On the left-hand side of the plot is the total integrated ELIS current as a function of time. When the end-cell neutral beams are turned on 25 ms into the

plasma shot, the ELIS current decreases dramatically. Focusing on this period of enhanced axial confinement, Fig. 12 compares I_S, $I_\parallel$, $I_\perp^{NA}$ and I_T for the period from 20 to 35 ms. The term $I_\perp^{NA}$ is small over this period because the PPC plates are electrically isolated to ground at 10 kΩ. (For comparison, a similar shot with grounded PPC plates would yield several amperes of $I_\perp^{NA}$.) Over the period of hot electron buildup (0–26 ms), the calculated q dN/dt term is first positive (0–22 ms) and then, for a short time (22–26 ms), negative. The period with a negative value is presumably due to the constant volume used to calculate the buildup term. After this initial period, the positive q dN/dt term more than offsets the difference between the measured ionization source I_S and the (small) plasma losses so that the calculated I_T is *greater than* or equal to I_S. For this plasma shot at lower density, we have used a constant value of R = 12.0, which corresponds to the plasma parameters after 28 ms. From 26 to 28 ms, R may be greater because of molecular penetration to the core, and this actually brings I_S into better agreement with I_T. Estimates of the uncertainties in I_T for this case — which are due almost entirely to the plasma buildup term — are difficult to quantify. However, as seen in Fig. 12, even with rather substantial errors (of the order of 50%) in the buildup term, the particle balance equation can be satisfied with a small I^A over the period of density buildup.

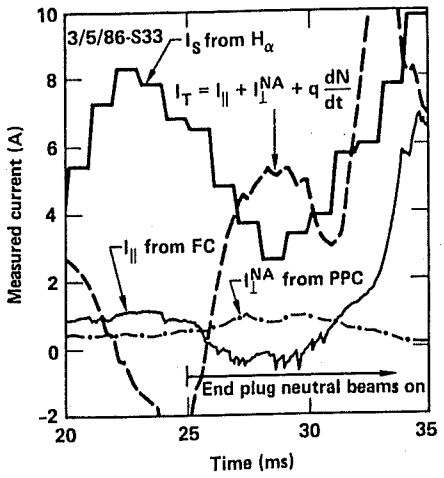

FIG. 12. Experimental Case 3: particle currents for the shot in Fig. 11 shown on an expanded time-scale. The axial ion losses $I_\parallel$ and the radial non-ambipolar losses $I_\perp^{NA}$ are small, starting at 25 ms. The particle buildup q dN/dt is the largest term in I_T after 25 ms. From 25 ms to about 30 ms, I_T is greater than or equal to the measured ionization source I_S, indicating small I^A. The total particle confinement time (assuming all losses originate in the central cell) is approximately 15 ms.

5. DISCUSSION OF PARTICLE CONFINEMENT TIMES IN TMX-U

Converting the measured particle currents to particle confinement times provides a convenient performance benchmark for tandem mirror operation. This conversion is normally based on a modification of Eq. (1), where each loss current is replaced by a term of the form qN/τ (e.g. $I_\parallel = qN/\tau_\parallel$), where τ is the particle confinement time. Of primary interest is the central-cell confinement time, because the central cell is the fusion producing region of a tandem mirror reactor. However, to calculate *only* central-cell confinement quantities, we must know the origin of the particle loss currents measured at the end walls, since the radial and axial losses in Eq. (1) may occur either in the central cell or in the end cells, or in both; we have measured only the total loss. These separate particle flows have been estimated, but a complete description is outside the scope of the present discussion [26]. For many conditions, however, it is found that the majority of the losses originate in the central cell. For this reason, a frequent *convention* is to assume that all of the particle currents originate in the central cell. This yields a pessimistic estimate of the central-cell confinement time (i.e. $\tau \doteq q\,N_{CC}/I$, where N_{CC} is the total number of central-cell particles). When this definition is used, the usual range of values observed in TMX-U is: $\tau_\parallel > 50$–100 ms, $\tau_\perp^{NA} > 20$ ms, and the ambipolar radial confinement time can be greater than or equal to the non-ambipolar radial confinement time. The best simultaneous values on one shot are: $\tau_\parallel \simeq 100$ ms, $\tau_\perp^{NA} \geq 15$ ms, and, since τ^A is long, the total confinement time is approximately 15 ms. During this period of enhanced confinement, the ionization time of 5 ms (derived from I_S) agrees with the plasma buildup time (derived from q dN/dt) of 5 ms. Although long axial [4] or radial [8] confinement times have been achieved previously in separate experimental runs on TMX-U, these are some of the best simultaneous parameters to date.

6. CONCLUSION

We have presented the first absolute measurements of the ionization source in a tandem mirror plasma. When these are compared with the measured particle losses and the density buildup, we are able to determine the magnitude of ambipolar transport. Under most conditions, I^A is small in the plasma core ($r \leq 10$ cm), but we have identified conditions in

which finite I^A is present. A low frequency density fluctuation (7 kHz) is often present when finite I^A is observed. Experimental measurements show that the ionization source is highly localized near the central-cell gas box, in agreement with DEGAS modelling predictions. In general, the DEGAS predictions agree with the measured H_α emissions and the pressure to within about a factor of two.

Finally, it should be noted that preliminary calculations to extend the particle balance to the whole cross-section have also been completed. In this case, the largest unknown factor is the correction necessitated by the presence of molecules at the edge, which is sensitive to the local electron density and temperature. Since detailed density and temperature data are not available at the plasma edge, estimates from Langmuir probe data on typical shots have been used to calculate the atomic physics factor R in this region. Initial measurements indicate that the total particle balance (i.e. the particle current terms integrated to the limiter at 25 cm) is not as good as the particle balance in the core; the term I_T is often less than 50% of I_S. A two-dimensional imaging microwave interferometer is planned for use in TMX-U to decrease the measurement errors in the central-cell electron density, including measurements at the edge of the plasma. It is hoped that the planned improvements in the edge diagnostics will result in improved particle balance measurements, particularly during periods of good axial and radial confinement.

ACKNOWLEDGEMENTS

The authors would like to acknowledge the contributions of the TMX-U experimental team, especially R. Wood for his work with the camera systems, M. Brown for computer programming, J. Foote for ELIS data, and G. Dimonte for useful discussions.

This work was performed under the auspices of the United States Department of Energy by the Lawrence Livermore National Laboratory, under Contract No. W-7405-ENG-48.

REFERENCES

[1] COENSGEN, F.H., ANDERSON, C.A., CASPER, T.A., et al., Phys. Rev. Lett. **44** (1980) 1132.

[2] CORRELL, D.L., ALLEN, S.L., CASPER, T.A., et al., Nucl. Fusion **22** (1982) 223.

[3] BALDWIN, D.E., LOGAN, B.G., Phys. Rev. Lett. **43** (1979) 1318.

[4] GRUBB, D.P., ALLEN, S.L., CASPER, T.A., et al., Phys. Rev. Lett. **53** (1979) 783.

[5] CHO, T., ICHIMURA, M., INUTAKE, M., et al., in Plasma Physics and Controlled Nuclear Fusion Research 1984 (Proc. 10th Int. Conf. London, 1984), Vol. 2, IAEA, Vienna (1985) 275.

[6] DRAKE, R.P., HOOPER, E.B., KARMENDY, C.V., et al., Phys. Fluids **25** (1982) 2110.

[7] HOOPER, E.B., COHEN, R.H., CORRELL, D.L., et al., Phys. Fluids **28** (1985) 3609.

[8] HOOPER, E.B., BALDWIN, D.E., FOWLER, T.K., et al., Phys. Fluids **27** (1984) 2264.

[9] POST, R.S., GERVER, M., KESNER, J., et al., in Plasma Physics and Controlled Nuclear Fusion Research 1984 (Proc. 10th Int. Conf. London, 1984), Vol. 2, IAEA, Vienna (1985) 285.

[10] INUTAKE, M., CHO, T., ICHIMURA, M., et al., Phys. Rev. Lett. **55** (1985) 939.

[11] SIMONEN, T.C., ALLEN, S.L., BALDWIN, D.E., et al., in Plasma Physics and Controlled Nuclear Fusion Research 1984 (Proc. 10th Int. Conf. London, 1984), Vol. 2, IAEA, Vienna (1985) 255.
ALLEN, S.L., BALDWIN, D.E., BARTER, J.D., et al., TMX-U Final Report, Rep. UCID-20981, Lawrence Livermore National Laboratory, Livermore, CA (1987).

[12] SIMONEN, T.C., ALLEN, S.L., CASPER, T.A., et al., Phys. Rev. Lett. **50** (1983) 1668.

[13] ALLEN, S.L., TMX-U Experimental Team, Rev. Sci. Instrum. **56** (1985) 873.

[14] GRUBB, D.P., Rev. Sci. Instrum. **56** (1985) 947.
SIMONEN, T.C., ALLEN, S.L., BALDWIN, D.E., et al., in Plasma Physics and Controlled Nuclear Fusion Research 1986 (Proc. 11th Int. Conf. Kyoto, 1986), Vol. 2, IAEA, Vienna (1987) 231.

[15] HEIFETZ, D., POST, D., PETRAVIC, M., WEISHEIT, J., BATEMAN, G., J. Comput. Phys. **46** (1982) 309.

[16] YU, T.L., ALLEN, S.L., MOOS, H.W., J. Vac. Sci. Technol. **3** (1985) 1077.

[17] FOOTE, J.H., COUTTS, G.W., PEDROTTI, L.R., SCHLANDER, L., WOOD, B.E., Rev. Sci. Instrum. **56** (1985) 1117.

[18] FOOTE, J.H., MOLVIK, A.W., TURNER, W.C., Rev. Sci. Instrum. **54** (1983) 928.

[19] STAIR, R., JOHNSTON, R.G., HALBACH, E.W., J. Res. Natl. Bur. Stand., A **64** (1960) 291.

[20] JOHNSON, L.C., HINNOV, E., J. Quant. Spectrosc. Radiat. Transfer **13** (1973) 333.

[21] McNEILL, D.H., BELL, M.G., GREK, B., LEBLANC, B., Edge Region Hydrogen Line Emission in the PDX Tokamak, Rep. PPPL-2085, Princeton Plasma Physics Laboratory, Princeton, NJ (1984).

[22] ALLEN, S.L., CLOWER, C., DRAKE, R.P., et al., J. Vac. Sci. Technol., A **1** (1983) 916.

[23] HILL, D.N., personal communications (1986).
ALLEN, S.L., KAISER, T.B., HILL, D.N., PICKLES, W.L., CORRELL, D.L., HEIFETZ, D.B., Bull. Am. Phys. Soc. **31** (1986) 1618.

[24] PICKLES, W.L., HUNT, A.L., J. Vac. Sci. Technol. **4** (1986) 1732.

[25] CASPER, T.A., personal communications (Nov. 1986).

[26] CORRELL, D.L., ALLEN, S.L., BROWN, M.D., Bull. Am. Phys. Soc. **30** (1985) 1429.

(Manuscript received 2 April 1987
Final manuscript received 13 August 1987)